Contractile Vacuole and Papilla drive Cyst/Telotroch transition in *Vorticella microstoma*

Author names.

Eric Galiana, Marie-Line Kuhn, Agnès Attard

Affiliations.

Université Côte d'Azur, INRAE, CNRS, ISA, Sophia Antipolis, France.

Corresponding author.

Eric Galiana, eric.galiana@inrae .fr

Present/permanent address

Institut Sophia Agrobiotech, 400 route des chappes, BP 167, 06903 Sophia Antipolis Cedex FRANCE

ASTRACT

The cyst of the protist ciliate Vorticella efficiently differentiates into teletroch, the free-swimming stage. Here, using video microscopy and quantitative imaging we establish that the cyst differentiation follows two strict temporal and spatial patterns. The temporal pattern is initially marked by the functional formation of the contractile vacuole, which then discharges its fluid into the neoformed cytopharynx and, in a third stage, into a membrane invagination which, to the rhythm of the vacuole, differentiates into an oral cavity exhibiting a polarized cilia array revealed by α-tubulin immunostaining. Two poles delineate the spatial pattern. The apical pole is defined by the position of the pre-existing papilla, which determines the site of oral cavity formation directly below it. The second basal pole is placed at the rupture point of the cyst wall. It is characterized by β-actin accumulation and allowed release of the telotroph according to its basal-apical polarity. Both the temporal and spatial patterns are impaired by concanamycin A treatment, a specific inhibitor of vacuolar type H^+-ATPases altering functions of contractile vacuoles. The findings indicate that cyst to telotroch transition is predetermined by the location of the papilla on the cyst wall and under the control of a functional contractile vacuole. We propose that *Vorticella* cyst is a simple single-cell model for investigating basic principles of integrative neogenesis of organelles in Protozoa, and of apical-basal cell polarity in Eukaryotes.

INTRODUCTION

Van Leeuwenhoek (1677) observed with his light-refracting lens microscope the first microbes, presumably a *Vorticella*. He described them as poor little creatures living in rainwater, having a round or oval body, moving or harpooning themselves towards the extremity, where they possess a contractile tail (stalk), and clumping together in a few filaments. The *Vorticella* genus is now a gathering of more than 100 different sessile peritrich ciliates (Sun et al, 2013). They evolve in marine, freshwater and terrestrial environments, moving or being attached to various substrates such as plant/animal surfaces and appendages, biofilms, flooded objects (Liao *et al.*, 2018; Galiana *et al.*, 2011; Davis and Gloege, 2024). They have been characterized as dominant protozoan species putatively playing a role in fertilization on N supply in rhizosphere soil during the initial growth of *Beta vulgaris L.* (Zeng *et al.*, 2020), and as potential biocontrol agents against plant-parasitic nematodes (Rostami *et al.*, 2022).

At the cellular level, they develop at least in three single-cell forms: free-swimming telotrochs, sessile stalked trophonts and cysts, the last ones being formed under adverse environmental conditions such as lack of nutrients or oxygen, drought, osmotic stress and extreme temperatures (Finley and Lewis, 1960; Bramucci and Nagarajan, 2004; Ryu *et al.*, 2017). The free-swimming telotroch (0.2-1 mm/s in speed) has generally an inverted bell-shaped morphology with an apical part surrounded by at least two rings of cilia emerging from the peristome, which surrounds the open oral cavity/mouth. Immediately behind, the cytopharynx, resulting from a plasma membrane invagination, connects together the oral cavity, particularly, to the food vacuoles, the digestive organelles, as well as the single contractile vacuole (CV). The osmoregulatory CV presumably emptying its contents into the cell's cytopharyngeal region through an elongated tube (Allen and Naitoh, 2002). The cell show the presence of a micronucleus and a polylobar macronucleus and the other eukaryotic organelles. The trophont sessile form has the same morphology and exhibits a retractile stalk (100-150 µm) with which the cell is attached to a surface. The water vortex flow generated by oral cilia beating results in drawing bacteria food particles toward the peristome and then to food vacuoles ingesting particles using phagocytosis. *Vorticella* species with their trophont-stalk contracting almost instantly (10-20 mm/s) and the high swimming speed (0.2-1 mm/s) of

69 the free telotroph are among the fastest cellular micromachines making them highly attractive
70 models for studying movements from hydrodynamic, cellular and molecular point of views
71 (Kamiguri et al, 2012; Ryu *et al.*, 2017; Lisicki et al, 2019; Lupatelli *et al.*, 2023).

72 Perhaps because cyst formation is a slower process, the dynamics of encystment occurring
73 upon adverse conditions, and excystment, allowing telotroch release from the cyst, are less
74 documented. (Warren, 1986). Cyst formation results to the formation of an envelope, the cyst
75 wall, encapsulating a diffuse cytoplasm/hyaloplasm with indistinct cilia, peristome,
76 cytopharynx and vacuoles. Upon favourable conditions, excystment is induced and
77 characterized by cyst differentiation, functional cilia and CV, with osmolarity as a main
78 regulatory factor (Finley and Lewis, 1960).

79 In protists, osmoregulation is achieved by CV which maintains osmotic and ion homeostasis
80 (Plattner, 2013, 2015; Jimenez *et al.*, 2022; More *et al.*, 2024). The cycle of CVs involves three
81 sequential events: diastole (slow extension of the vacuole gradually filled with excess water
82 drained into the endoplasm); systole (rapid vacuolar contraction); and expulsion (the release
83 of vacuolar fluid from the CV outside the cell). To maintain osmotic and ion homeostasis
84 through extrusion of water and excess of ions, the CV may exploit the H^+-gradient generated
85 by the organelle-resident Vacuolar ATPases (V-type H^+-ATPase) (Patterson, 1980; Plattner,
86 2013, 2015). The V-ATPase is highly conserved in eukaryotic organisms and is assembled into
87 two structural multimeric protein complexes: a transmembrane V0-proton pump and a
88 cytoplasmic V1-ATPase that can be reversibly detached and reattached (Wassmer *et al.*, 2006;
89 Wang *et al.*, 2020). In protists as *Dictyostelium* and *Phytophthora* (Temesvari et al, 1996;
90 Mitchell and Hardham, 1999) the function of vacuolar contraction is impaired by
91 concanamycin A, a specific inhibitor of V-ATPases, binding to the V0 subunit c (Huss et al,
92 2002).

93 To date and for a long time ago, knowledge of the *Vorticella* cyst still remains meagre (Warren,
94 1986). The underlying machinery controlling encystment and excystment remains unexplored
95 since the first study of Finley and Lewis (1960). Here, we combine quantitative imaging with
96 drug-inhibited V-ATPase activity to characterize the dynamics of excystment and telotroch
97 release from the *Vorticella microstoma* cyst induced in response to hypo-osmotic conditions.
98 We established that before release, oral cavity and cilia neogenesis, as well as cyst wall
99 deformation follow the redifferenciation of the CV and that their formation is tightly

synchronised both spatially and temporally with the acceleration of the pulsatile rhythm of the diastole-systole-expulsion sequence. We show that inhibition of V-ATPase-mediated proton pumping causes drastic deficits in telotroch release, speed motion as well as cilia organisation and distribution. We propose that *Vorticella* cyst is a simple model for investigating basic principles of integrative neogenesis of organelles in Protozoa, and of basal-apical cell organisation in eukaryotes.

RESULTS

Excystment main features

Encystment and excystment have been reported in several ciliated protists (Li et al, 2022; Jin *et al.*, 2024), in few species within the *Vorticella* genus (Warren, 1986) among which *V. microstoma* (Finley and Lewis, 1960) that was investigated in this work. Encystment was induced at a rate of 100% after incubation of *V. microstoma* cells in V8 medium in long-term-culture (10–14 days). At these time-points of incubation, no trophont nor telotroph could be detected with binoculars. The dynamics of encystment was not further examined in this study. To further study the dynamic of excystment, we applied a hypo-osmotic shock to this cyst population. In these conditions, the rate of excystment was estimated at 30% to 50% within 1-2 hours. At this time, microscopic observations allowed to establish that the cell released were telotrophs either swimming freely or not. Further investigation on excystment dynamics focused on telotrophs that were not yet swimming and were almost exclusively localized immediately adjacent to the empty cyst wall from which each had emerged. In the results that follow, the timing assigned to each event described refers to the moment (t=0) when osmotic stress was applied.

Just before the stress, all *Vorticella* material consisted of perfectly circular and encapsulated cysts (⌀28.8±0.9 µm) with a papilla located at one of its poles as illustrated in Fig. 1A and 1B. At this time (t=0), an immunostaining for the α-tubulin subunit revealed an intracellular and diffuse staining homogeneously distributed in the cytoplasm, suggesting that microtubules were not or poorly polymerised and cilia resorbed (Fig. 1B). Around t=30 min, re-differentiation was initiated as attested by the formation of the contractive vacuole (Fig. 1C) and the cytoplasmic staining for α-tubulin which became punctuated indicating αβ-tubulin oligomerisation in clusters (Fig. 1D). From around t=30-60 min, telotroch release from cysts took place in number. The turgor pressure generated by the telotroph size increase stretched the cyst wall to its maximum capacity up to a breaking point. Cells exhibited the characteristic telotroch bell morphology decorated by cilia (Fig. 1E and 1G). As previously described, their size (1595,5 ± 58,8 μm^2) was significantly increased (p=0,0005; n=14) by 2,4 times compared to cysts (571,2±36,9 μm^2).

136 Immunostainning for α-tubulin (Fig. 1F and 1H) clearly showed occurrence of microtubule
137 polymerisation and cilia neogenesis at the apical side (the oral mouth) of the telelotroph (Fig.
138 1E and 1G), and at its basal side (Fig. 1G). The rupture point of cyst wall at release was detected
139 at the opposite side of the papilla when this one was visible in the plan (Supplementary Fig.
140 1). The position of this point was inscribed in the half-circle opposite to the location of the
141 papilla. This indicated that at the time of rupture, the pressure is exerted differently along a
142 particular cellular axis. Another interesting point is congruent with this hypothesis:
143 systematically, the release of the cell took place according to its apical-basal polarity, its basal
144 end engaging first (Supplementary Fig. 1).

145

146 *Tracking early organelles neogenesis*

147 To examine more precisely, the spatio-temporal dynamics of organelles neogenesis (contactile
148 vacuole, oral mouth, cytopharynx, cilia, cyst wall deformation) within the cyst, samples were
149 positioned in the chamber just after the hypo-osmotic stress. Cysts and excystment were
150 captured at 5 frames per second until telotroch release (Fig. 2; movies 1, 2 and 3). The time
151 series images were processed by kymography. Figure 2 summarises the occurrence of
152 sequential events observed.

153 For the CV, we retrieved from kymograms the number of pulsations before release, kinetics
154 of beating frequency, size of the vacuole at the end of systole (Fig 3). The data show that the
155 time point of the first pulse was variable and detectable quite a long time [7-21 min range]
156 after stress induction (Fig. 3A,B). The total number of pulse before release was constant (41±4,
157 Fig. 3C). Within a range between 0,01 and 0,05 Hz, the contractile frequency distribution
158 overtime reveals for all samples the same pattern: first slow pulsations with a progressive
159 increase in pulse frequencies and then a decrease for the last 5 to 10 ones before release (Fig.
160 3D and Supplementary Fig. 2). These variations are mainly due to variability in diastole
161 duration, while the duration of each systole appears to be very short and constant, estimated
162 in these experiments at 0.8-1 s. As illustrated in Fig 3A, the CV increased in size with time
163 reaching its maximal volume just before release. The overall size was not quantified with
164 kymographic data because vacuole position related to the selected line along the diameter
165 could change marginally due to low flow or Brownian motion acting on the cyst. Changes in

166 vacuole diameter size were manually quantified at three steps: at the first (C_f) and last (C_l)
167 pulse detected within cyst and immediately after release within telotroph (T) (Fig. 3E). At C_l,
168 diameter was approximately 1,9 ($\pm$0,5)-fold larger than at C_f, and 1,6 ($\pm$0,4)-fold larger at T
169 than at C_l. Thus, we can approximate that during differentiation from cyst to telotroch the
170 volume of the CV increased 15 to 20-fold time.

171 Cytopharinx neogenesis was difficult to date precisely. However, when cytopharinx structures
172 were first visualized in several successive time lapse sequences they clearly appeared only in
173 correlation with the ability of vacuole to contraction (movie 1, 2 and 3). Moreover, part if not
174 all the vacuole fluid discharge flew into the cytopharinx at systole. Indeed cytopharyngeal
175 volume began to increase on the same frame on which for the first time at the end of diastole,
176 systole started as attested by the decrease of the vacuole volume (Fig. 2A-B and Fig. 4). This
177 increase reached its maximum in the same range of systole duration 0.8-1,2 s (Fig. 4A-D) even
178 if here, the frequency of image acquisition did not allow a finer temporal resolution of these
179 two rapid events.

180 Remarkably, our refined temporal analysis also revealed that oral cavity/mouth arise from a
181 thin sheet, that could correspond to a plasma membrane invagination, whose expansion was
182 cadenced by the vacuole contraction (Movie 1, 2 and 3). This primitive thin sheet is first
183 visualized within the hyaloplasm directly and always beneath the papilla (Fig. 2C; Movie 1),
184 probably involving a specialized cell cortex area for anchorage. At this stage, no cilia are visible
185 and appear neither formed nor functional. The sheet gradually individualizes by rhythmic
186 expansion, evolving into a cavity under successive repetitions of vacuole pulsations. The
187 vacuole might empty its fluid into the cytopharyngeal region which joins the oral cavity by
188 forming a tube (Movie 1). It is also noteworthy to note that when a kymogram was drawn
189 based on a section line crossing organelles from the papilla to the vacuole (Fig. 5A, B), the oral
190 cavity enlargement timely and perfectly coincided with the diastole/systole transition (Fig.
191 5C). The progressive enlargement could only be detected at the late stages of differentiation.
192 At these stages, the emergence of cilia was detected as shown in Figure 2E-2F, and by the
193 perceptible cilia vibration as the cavity expands just before and after release (Movie 1 and 3).
194 Once formed, this cavity constitutes the oral mouth which appears to remain closed
195 throughout the cyst differentiation-telotroch differentiation sequence.

196

197 *Deformation and rupture of cyst wall*

198 At latest stages of cyst differentiation, cyst wall deformation was initiated over a long and
199 variable time [10-200s] before release (Fig. 6A). Sequence images analysis revealed that the
200 cyst wall firstly underwent plastic deformation and then rupture. The plastic deformation
201 exerted all along this time while the rupture was not quantified since it occurred in less than
202 0.2 s, the resolution time of the movies. Plastic deformation resulted from a protrusion at the
203 leading edge taking place in an angular position located in the semi-circle opposite to the
204 papilla coordinates (Fig. 6B) positioning the rupture point for the telotroph release which will
205 follow (Supplementary Fig 1). The plastic deformation resulted with time in an increase in the
206 perimeter of the cyst (Fig. 6C) that could reach just before release 24,2±7,9 µm (Fig. 6D)
207 illustrating the significant elastic/elongation properties of polymers of the cyst wall.
208 Deformation and rupture of cyst wall were associated with local β-actin accumulation
209 revealed by immunostaining just before (Fig. 6 E-G) or during release (Fig. 6 H-J) suggesting
210 that protrusion at the leading edge requires actin filament recruitment.

211

212 *Concanamycin A inhibits cyst differentiation and telotroch release*

213 To initiate exploration of machinery controlling excystment, we assessed the function of the
214 CV complex, the first organelle formed and that seemed involved in cytopharinx and oral
215 mouth neogenesis. The investigation was focused on the V-ATPases generating H^+-gradient
216 across membranes. The V-ATPases are present in abundance in the CV membranes of different
217 protozoa living in a wide range of osmotic environments and important for vacuolar function
218 in expelling water entering the cells by osmosis (Allen and Naitoh; 2002). We first checked if
219 V-ATPases were localized at the CV. We proceeded by immunostaining of cysts and teletroch
220 with a polyclonal antibody against the B1-subunit of the V1-ATPase subcomplex. The results
221 established that in *Vorticella* as in other protists these proteins are plasma and vacuolar
222 membrane-resident (Fig. 7A-D). The typical cressent-like staining of a single vacuole among
223 the food vacuoles and the contractile one strongly indicated that the antibody decorated
224 membranes of the CV. Next, we examined the action of the concanamycin A, a specific
225 inhibitor of the V-ATPases, on cyst differentiation and release. Cysts in stationary phase were
226 collected, washed and then incubated in water in the presence or not of 5 µM concanamycin

227 A. We therefore examined the action of the drug on the function of the CV complex in cyst
228 differentiation and release based on counting in each condition both (i) filled and versus
229 empty cyst walls to calculate the ratio between empty and total cysts numbers (Fig. 7E); and
230 (ii) mean speed of telotrophs in motion (Figure 7F). As expected, no empty cyst wall was
231 detected in cysts at stationary phase (SP; 14-day culture in V8 medium) while a high rate for
232 empty cyst walls was calculated in the control (C) after one hour of release in water. In contrast
233 and at the same time point, in concanamycin A-treated samples (Conca A) the rate of empty
234 cysts was drastically reduced compared to control cells (Fig. 7E). Concomitantly, there was
235 also a marked decrease in the mean speed of moving cells in the presence of the drug (Fig. 7F)
236 indicating that cysts were impaired in the differentiation and/or release processes. Next, we
237 visualized α-tubulin by immunostaining. In the control cells, the α-tubulins were mainly
238 distributed at the two poles of most released telotrochs (Fig. 7G) drawing the characteristics
239 two ciliary arrays of *Vorticella* sp. which promote fluid flow for cell motility; In the
240 concanamycin A-treated cells, cysts and telotrochs were faintly stained compared to the
241 control cells (Supplementary Fig. 3 A,B). The telotrochs could exhibited a staining more
242 uniformly distributed and not reminiscent to a clear polarized status indicating that
243 ciliogenesis, involving polarized basal body docking onto cell membranes, were inhibited or
244 slowed (Fig. 7G). A larger CV could also be observed with an extended systole and no structure
245 reminiscent to the cytopharingal cavity nor ciliated oral mouth (Supplementary Fig. 3, H-L).

246

247 **DISCUSSION**

248 There is today a real Vorticella paradox. Although it was probably the first microorganism
249 described in detail (Van Leeuwenhoek, 1677), *Vorticella sp.* remains a "poor little creature"
250 being among the most neglected organisms in terms of available data in cellular and molecular
251 Biology and Genomics. Only 328 nucleic acid and 9 protein sequences are accessible in
252 databases such as NCBI or Uniprot. It seems not to have yet appeared in the Protist 10 000
253 Genomes Project (Gao *et al.*, 2024). And yet, its distinctive single-celled forms (cyst, telotroph,
254 trophont) make them really suitable objects of investigation on the mechanisms that govern
255 biological transitions within a species. Using microscopy and pharmacology, the current study
256 explored the cyst-telotroph transition in the ciliate Vorticella allowing to excystment.

257 *The cyst excystment of the Vorticella ciliate*

258 (Li *et al.*, 2022) have reviewed a vast amount of information available on changes and some
259 known mechanisms involved during excystment process of 14 representative ciliated protists.
260 General principles on which excystment is induced involved first reappearance of ciliary and
261 intracellular structures that had degenerated during encystment and before excysting.
262 Second, escape from the cyst wall is assisted by a preformed or neoformed pore on the cyst
263 wall and a rupture generated by the pressure of cell movement inside the cyst wall and
264 excystation vacuole. In *Pleurotricha lanceolate,* generation of the pore occurred at uncertain
265 position (Jeffries, 1956).

266 In the current study the data indicate that the papilla and the CV orchestrate a complete
267 differentiation in telotroch from a cyst initially constituted of unstructured
268 hyaloplasm/cytoplasm. They allow us to define two patterns characterizing the cyst transition
269 to telotroph. A first temporal pattern is initially marked by the functional formation of the CV,
270 which then discharges its fluid into the neoformed cytopharynx and, in a third stage, into a
271 membrane invagination which, to the rhythm of the vacuole, differentiates into an oral cavity.
272 The second pattern, a spatial one, is delineated on one pole by the position of the papilla,
273 which determines the site of oral cavity formation and ciliogenesis, directly below it and
274 dictated by the CV tempo. The point of cyst wall rupture, leading to the release of the telotroch
275 in an apical-basal polarity defines the second pole and is characterized by β-actin

accumulation. The data emphasizes the role of CV and papilla in the two axes setting up (Fig. 8).

Indeed, two lines of evidences designate the CV if not the conductor of the establishment of the first temporal pattern, at least as a key upstream player. (i) It is the first functional organelle to emerge. At the strict tempo of its contractions, the appearance of the cytopharynx and then the oral mouth sequentially follow. (ii) Concanamycin A treatment compromising its V-ATPase-dependent functions alters ciliogenesis, polarized ciliary arrangement, release and motion of telotrochs. CV could act by regulating osmotic and ion homeostasis as suggested by the increase in size of released telotroph compared to cyst. It could also act by discharging signaling molecules to the plasma membrane of nascent organelles (cytopharynx , oral mouth), *as D. discoideum* CV discharges cAMP and Ca^{2+} to plasma membrane at the rear of each cell during early cell aggregation allowing stalk formation (Fadil and Janetopoulos, 2021).

A passive but key player in the spatial pattern definition is clearly the papilla. Its position initially defines the plasma membrane anchored one where oral mouth will emerge precisely positioned neatly under the papilla. By this way it determines the position of the apical-basal polarity of the neoformed telotroph. Considering that the release always occurred according to the basal-apical polarity of telotroph and within the semi-circle opposite to the papilla, papillae must be considered as the organisers establishing the spatial pattern of excystment. Thus, a papilla position is a reference point of a developmental process and not a simple morphological ornament precious for taxonomy.

Morphogenesis of apical-basal polarity

More broadly, telotroch differentiation in Vorticella should also be a new model to investigate the apical-basal polarity that is essential to many morphogenetic processes in eukaryotes. Its establishment is extensively studied at the genetic and molecular level in higher eukaryotes (Motegi *et al.*, 2020), in ciliates (Soh and Pearson, 2022) or amoebozoa as the unicellular *D. discoideum* (Fadil and Janetopoulos, 2021). In *Vorticella* the establishment of apical-basal polarity is achieved within the cyst before release and simply results of a single-cell process primary involving the same two structures, the generative CV and the positional papilla. The pre-existing papilla of the cyst wall is a structural constraint defining the position of the apical

306 organization of future telotrophs through attachment of a particular cortical area of the
307 plasma membrane from which emerges the oral cavity. This could be view as an additional
308 facet of "structural inheritance" whereby in ciliates pre-existing structures enforce a
309 developmental plan for newly formed structures (Beisson & Sonneborn, 1965). In
310 *Tetrahymena pyriformis* and *Paramecium tetraurelia*, the pre-existing intracellular cortical
311 organization of cilia deliver information for the formation and positioning of new structures
312 (basal bodies, microtubular network) defining the cortical organization after scission (Beisson
313 & Sonneborn, 1965; Ng and Frankel, 1977; Soh and Pearson, 2022). It is also reminiscent to
314 maternal tissues acting in higher eukaryotes as a mechanical constraint (Woudenberg *et al.*,
315 2024) as the cell wall-mediated maternal control of apical–basal patterning in brown algae
316 (Shaw and Quatrano, 1996; Dries *et al.*, 2024). The present data clearly indicate that in
317 *Vorticella*, the papilla constitutes the extracellular anchorage point for cellular material
318 assembled during encystment and pre-required for oral cavity and cilia array formation during
319 excystment. Such material could include the fibrillary one viewed after release in Fig. 2F and
320 Movie 1, still linked at the papilla site after release, and conforming to the shape of the thin
321 sheet forming beneath the papilla (Fig2C). The establishment of apical-basal polarity also
322 involves a functional generative CV complex. The analyses of the movies clearly establish that
323 CV expels its fluid through the pore in the cytopharynx. The discharge is then mainly
324 propagated until the papilla-located thin sheet contributing to oral cavity and cilia array
325 formation. The discharge wave did not propagate to the rest of the cell which constitute
326 schematically below the vacuole, the basal side of the cell. Thus cellular process that is
327 happening, it is as though fluid discharge defines a developmental apical way from the CV to
328 the papilla on which cytpharynx and oral mouth genesis take place.

329 *Conclusion*

330 Encystment and excystment are fundamental to the conservation and dissemination of
331 protists in the biosphere. Most of the molecular and cellular associated mechanisms remains
332 elusive. We highlighted generative and structural elements that organise from a cyst and
333 according to a spatio-temporal plan the telotroch differentiation, apical-basal cell polarity and
334 excystment in the ciliate *Vorticella*. By the identification of the papilla as a positional
335 constraint and the CV as a generative organelle of cell polarity in a single-cell system, we
336 provide a new and additional evidence that apical-basal cell polarity is an ancestral trait not

337 only widespread among eukaryotic multicellular cell organisations. Future studies in cell
338 biology will be required to understand how the papilla is formed during encystment, which
339 cellular components are locally recruited to precisely mounted the site of oral cavity and apical
340 cilia array formation, and which CV function(s) (water exclusion, ion homeostasis, signaling
341 molecule driver) controls the cell differentiation.

342

343 **MATERIALS AND METHODS**

344 *Vorticella Strain and sample treatment*

345 The *Vorticella microstoma* 30897 stain, in co-culture with *Enterobacter aerogenes (*13048
346 strain), was purchased from the American Type Culture Collection (ATCC) collection of protists
347 (LGC standards). The cells were cultivated for 3 to 14 days in V8 liquid medium at 24°C. Three
348 days were necessary to observe a high rate of swimming telotroch. Ten to fourteen days were
349 required to reach a 100% rate for cyst formation. In the intermediate range of time, the
350 trophont appeared to be the most common form observed. To induce cyst excystment by
351 means of a hypo-osmotic stress, the medium of 10-14-day-old cultures was discarded and
352 cysts were resuspended in water (the time point t=0 in this study). Samples (100-200 µl) were
353 rapidly mounted in a chamber made of a microscope slides and a top coverslip loaded on two
354 spacers (0,5-1 mm) for starting microscopic observation soon as possible.

355 To inhibit the V-ATPase, cysts were treated with Concanamycin A, a specific inhibitor of V-
356 ATPases binding to the proteolipid subunit c of the V0 complex (Huss *et al.*, 2002). To assess
357 the function of the CV machinery we proceeded as previously described by Tesmesvari *et al.*
358 (1996) with *Dictyostelium discoideum*. Cysts in the stationary phase were harvested by
359 centrifugation, resuspended in water to create a hypo-osmotic environment and treated or
360 not with 5µM Concanamycin A in solution in DMSO. The appropriate DMSO dilution was
361 applied to the control samples.

362

363 *Microscopy*

364 Images (size 512×512 or 1029x1044 pixels) and movies (image 512×512 pixels; time scale 0.2
365 or 0,4s; time series 1000-3000 s) were obtained using a Zeiss Axio Z1 microscope equipped as
366 followed : a plan-apochromat63x/1.40oil M27 and a EC-plan-neofluofluar 40x.75 M27
367 objectives; a Hamamatsu camera and the ZEN 2012 pro lite application (Carl Zeiss Microscopy,
368 Germany). The material was available on the Microscopy Platform-Sophia Agrobiotech
369 Institut-INRAE 1355-UNS-CNRS 7254-INRAE PACA, Sophia Antipolis.

370

371

372 *Immunohistochemistry*

373 Cysts and telotrochs were collected by centrifugation. They were fixed in methanol for 10 min
374 at -20°C and then incubated in phosphate-buffered saline (PBS), pH 7.2 at room temperature.
375 Samples were treated in PBS with 0,1% Triton for 20 min at room temperature, and later with
376 a blocking solution containing 3% of bovine serum albumin in PBS, for 30 min. They were then
377 first incubated for 18h at 4°C with a rabbit polyclonal antibody against the α-tubulin subunit
378 (NeoBiotech), or against the V1-ATPase B1 subunit (NeoBiotech), or against the β-actin diluted
379 1:200. Samples were washed three times with PBS and incubated for 1 h at room temperature
380 with a FluoProbes 547H Donkey anti-Rabbit IgG or a Fluoprobes 488 anti-rabbit IgG antibody
381 diluted 1:200 (Interbiotech – BioScience Innovations). Samples were rinsed three times and
382 mounted in Fluoroshield with DAPI (Sigma, St. Louis, MA USA).

383

384 *Image time series analysis*

385 To analyse CV beating, cytopharynx and oral mouth expansion we proceeded by kymography
386 using in FIJI (Schindelin *et al.*, 2012) the Measurement_Tool plugin (k-button;
387 https://dev.mri.cnrs.fr/projects/imagej-macros/wiki/Velocity_Measurement_Tool). To
388 generate the kymograms, we applied the tool by selecting segmented lines including a
389 diameter and the centre of the vacuole or delimiting as much as possible the mid-section of
390 the papilla, oral cavity, cytopharynx and contractile vacuole. In the kymograms, space was
391 measured along the x-axis while time was measured along the y-axis. To determine mean
392 velocity of cysts and telotrochs, cells were tracked with FIJI using the TrackMate plugin (Ershov
393 *et al.*, 2022) as per the procedure detailed in Lupatelli *et al.* (2023).

394 *Statistics*

395 Experiments were repeated at least 3 times. Data are presented as mean values±SEM. One-
396 way ANOVA with Mann-Whitney pairwise test, were used for the statistical analysis. Past4.17
397 software was used to analyse the data. Bonferroni corrected/adjusted p values of <0.05 are
398 indicated and were considered.

399

400 **Funding**

The work was supported by the National Research Agency; project number ANR22-CE20-0021.

Author contributions

EG and MLK conducted the analyses. EG wrote the first draft. AA and MLK contributed to the writing of the manuscript. EG and AA managed acquisition of the financial support for the project leading to this publication.

Acknowledgements

A warm thank-you goes to Carlotta Aurora Lupatelli for very fruitful discussions on the topic of the paper.

412 **REFERENCES**

413 Allen, R. D., and Naitoh, Y. (2002). Osmoregulation and contractile vacuoles of protozoa. Int
414 Rev Cytol 215, 351–94. https://doi.org/10.1016/s0074-7696(02)15015-7

415 Beisson, J., and Sonneborn, T. M. (1965). Cytoplasmic Inheritance of the Organization of the
416 Cell Cortex in *Paramecium Aurelia*. Proc Natl Acad Sci U S A 53, 275–82.
417 https://doi.org/10.1073/pnas.53.2.275

418 Bramucci, M. G., and Nagarajan, V. (2004). Inhibition of Vorticella microstoma Stalk Formation
419 by Wheat Germ Agglutinin. J Eukaryot Microbiol 51, 425–427. https://doi.org/10.1111/j.1550-
420 7408.2004.tb00389.x

421 Davis, A. K., and Gloege, H. (2024). Ciliated Epibionts Modify the Cardiac Stress Reaction to
422 Perceived Predation in Daphnia. Microorganisms 12.
423 https://doi.org/10.3390/microorganisms12061219

424 Dries, E., Meyers, Y., Liesner, D., Gonzaga, F. M., Becker, J. F. M., Zakka, E. E., *et al.* (2024). Cell
425 wall-mediated maternal control of apical–basal patterning of the kelp *Undaria pinnatifida*.
426 New Phytologist 243, 1887–1898. https://doi.org/https://doi.org/10.1111/nph.19953

427 Ershov, D., Phan, M. S., Pylvanainen, J. W., Rigaud, S. U., Le Blanc, L., Charles-Orszag, A., *et al.*
428 (2022). TrackMate 7: integrating state-of-the-art segmentation algorithms into tracking
429 pipelines. Nat Methods 19, 829–832. https://doi.org/10.1038/s41592-022-01507-1

430 Fadil, S. A., and Janetopoulos, C. (2021). The Polarized Redistribution of the Contractile
431 Vacuole to the Rear of the Cell is Critical for Streaming and is Regulated by PI(4,5)P2-Mediated
432 Exocytosis. Frontiers in cell and developmental biology 9, 765316.
433 https://doi.org/10.3389/fcell.2021.765316

434 Finley, H. E., and Lewis, A. C. (1960). Observations on excystment and encystment of *Vorticella*
435 *microstoma*. J Protozool 7, 347–351. https://doi.org/10.1111/j.1550-7408.1960.tb05981.x

436 Galiana, E., Marais, A., Mura, C., Industri, B., Arbiol, G., and Ponchet, M. (2011). Ecosystem
437 screening approach for pathogen-associated microorganisms affecting host disease. Appl
438 Environ Microbiol 77, 6069–75. https://doi.org/10.1128/AEM.05371-11

439 Gao, X., Chen, K., Xiong, J., Zou, D., Yang, F., Ma, Y., *et al.* (2024). The P10K database: a data
440 portal for the protist 10 000 genomes project. Nucleic Acids Res 52, D747–D755.
441 https://doi.org/10.1093/nar/gkad992

442 Huss, M., Ingenhorst, G., König, S., Gassel, M., Dröse, S., Zeeck, A., *et al.* (2002). Concanamycin
443 A, the specific inhibitor of V-ATPases, binds to the V(o) subunit c. The Journal of biological
444 chemistry 277, 40544–8. https://doi.org/10.1074/jbc.M207345200

445 Jimenez, V., Miranda, K., and Augusto, I. (2022). The old and the new about the contractile
446 vacuole of *Trypanosoma cruzi*. J Eukaryot Microbiol 69, e12939.
447 https://doi.org/10.1111/jeu.12939

448 Jin, D., Li, C., Chen, X., Wang, Y., Al-Rasheid, K. A. S., Stover, N. A., *et al.* (2024). Decryption of
449 the survival "black box": gene family expansion promotes the encystment in ciliated protists.
450 BMC Genomics 25, 286. https://doi.org/10.1186/s12864-024-10207-3

451 Kamiguri, J., Tsuchiya, N., Hidema, R., Yatabe, Z., Shoji, M., Hashimoto, C., *et al.* (2012).
452 Contraction behaviors of *Vorticella* sp. stalk investigated using high-speed video camera. II:
453 Viscosity effect of several types of polymer additives. Biophysics (Nagoya-shi, Japan) 8, 11–19.
454 https://doi.org/10.2142/biophysics.8.11

455 Li, Y., Wang, Y., Zhang, S., Maurer-Alcalá, X. X., and Yan, Y. (2022). How Ciliated Protists Survive
456 by Cysts: Some Key Points During Encystment and Excystment. Frontiers in microbiology 13,
457 785502. https://doi.org/10.3389/fmicb.2022.785502

458 Liao, C. C., Shin, J. W., Chen, L. R., Huang, L. L. H., and Lin, W. C. (2018). First molecular
459 identification of *Vorticella* sp. from freshwater shrimps in Tainan, Taiwan. International
460 journal for parasitology. Parasites and wildlife 7, 415–422.
461 https://doi.org/10.1016/j.ijppaw.2018.10.002

462 Lisicki, M., Velho Rodrigues, M. F., Goldstein, R. E., and Lauga, E. (2019). Swimming eukaryotic
463 microorganisms exhibit a universal speed distribution. eLife 8.
464 https://doi.org/10.7554/eLife.44907

465 Lupatelli, C. A., Attard, A., Kuhn, M. L., Cohen, C., Thomen, P., Noblin, X., *et al.* (2023).
466 Automated high-content image-based characterization of microorganism behavioral diversity

467 and distribution. Comput Struct Biotechnol J 21, 5640–5649.
468 https://doi.org/10.1016/j.csbj.2023.10.055

469 Mitchell, H. J., and Hardham, A. R. (1999). Characterisation of the water expulsion vacuole in
470 *Phytophthora nicotianae* zoospores. Protoplasma 206, 118–130.
471 https://doi.org/10.1007/BF01279258

472 More, K. J., Kaur, H., Simpson, A. G. B., Spiegel, F. W., and Dacks, J. B. (2024). Contractile
473 vacuoles: a rapidly expanding (and occasionally diminishing?) understanding. European
474 Journal of Protistology 94, 126078. https://doi.org/10.1016/j.ejop.2024.126078

475 Motegi, F., Plachta, N., and Viasnoff, V. (2020). Novel approaches to link apico-basal polarity
476 to cell fate specification. Current Opinion in Cell Biology 62, 78–85.
477 https://doi.org/10.1016/j.ceb.2019.09.003

478 Ng, S. F., and Frankel, J. (1977). 180 degrees rotation of ciliary rows and its morphogenetic
479 implications in Tetrahymena pyriformis. Proc Natl Acad Sci U S A 74, 1115–9.
480 https://doi.org/10.1073/pnas.74.3.1115

481 Patterson, D. J. (1980). Contractile vacuoles and associated structures: their organisation and
482 function. Biological Reviews 55, 1–46. https://doi.org/10.1111/j.1469-185X.1980.tb00686.x

483 Plattner, H. (2013). Contractile vacuole complex–its expanding protein inventory. Int. Rev. Cell
484 Mol. Biol. 306, 371–416. http://dx.doi.org/10.1016/B978-0-12-407694-5.00009-2

485 Plattner, H. (2015). The contractile vacuole complex of protists--new cues to function and
486 biogenesis. Critical reviews in microbiology 41, 218–27.
487 https://doi.org/10.3109/1040841x.2013.821650

488 Rostami, M., Karegar, A., and Hamzehzarghani, H. (2022). Biocontrol Potential of the Vorticella
489 sp. Isolated from Vermicompost Against Meloidogyne javanica. Current microbiology 79, 333.
490 https://doi.org/10.1007/s00284-022-03030-0

491 Ryu S., Pepper R. E., Nagai M., and France D. C. (2017). Vorticella: a protozoan for bio-inspired
492 engineering. Micromachines 8 ,4. https://doi.org/10.3390/mi8010004

493 Schindelin, J., Arganda-Carreras, I., Frise, E., Kaynig, V., Longair, M., Pietzsch, T., *et al.* (2012).
494 Fiji: an open-source platform for biological-image analysis. Nat Methods 9, 676–82.
495 https://doi.org/10.1038/nmeth.2019

496 Shaw, S. L., and Quatrano, R. S. (1996). The role of targeted secretion in the establishment of
497 cell polarity and the orientation of the division plane in Fucus zygotes. Development
498 (Cambridge, England) 122, 2623–30. https://doi.org/10.1242/dev.122.9.2623

499 Soh, A. W. J., and Pearson, C. G. (2022). Ciliate cortical organization and dynamics for cell
500 motility: Comparing ciliates and vertebrates. J Eukaryot Microbiol 69, e12880.
501 https://doi.org/10.1111/jeu.12880

502 Sun, P., Clamp, J. C., Xu, D., Huang, B., Shin, M. K., and Turner, F. (2013). An ITS-based
503 phylogenetic framework for the genus *Vorticella*: finding the molecular and morphological
504 gaps in a taxonomically difficult group. Proc Biol Sci 280, 20131177.
505 https://doi.org/10.1098/rspb.2013.1177

506 Temesvari, L. A., Rodriguez-Paris, J. M., Bush, J. M., Zhang, L., and Cardelli, J. A. (1996).
507 Involvement of the vacuolar proton-translocating ATPase in multiple steps of the endo-
508 lysosomal system and in the contractile vacuole system of Dictyostelium discoideum. J Cell Sci
509 109 (Pt 6), 1479–95. https://doi.org/10.1242/jcs.109.6.1479

510 Van Leewenhoeck, A. (1677). Observations, communicated to the publisher by Mr. Antony van
511 Leewenhoeck, in a Dutch letter of the 9th of Octob. 1676. Philos. Trans. R. Soc. Lond. 12, 821–
512 831. https://doi-org.insb.bib.cnrs.fr/10.1098/rstl.1677.0003

513 Wang, L., Wu, D., Robinson, C. V., Wu, H., and Fu, T. M. (2020). Structures of a Complete
514 Human V-ATPase Reveal Mechanisms of Its Assembly. Mol Cell 80, 501-511 e3.
515 https://doi.org/10.1016/j.molcel.2020.09.029

516 Warren, A. (1986). A revision of the genus *Vorticella* (Ciliophora: Peritrichida). Bulletin of the
517 British Museum (Natural History) Zoology 50, 1–57. https://archive.org/details/biostor-
518 39/mode/2up

519 Wassmer, T., Kissmehl, R., Cohen, J., and Plattner, H. (2006). Seventeen a-subunit isoforms of
520 paramecium V-ATPase provide high specialization in localization and function. Mol Biol Cell
521 17, 917–30. https://doi.org/10.1091/mbc.e05-06-0511

Woudenberg, S., Hadid, F., Weijers, D., and Borassi, C. (2024). The maternal embrace: the protection of plant embryos. Journal of Experimental Botany 75, 4210–4218. https://doi.org/10.1093/jxb/erae071

Zheng, W. B., Wang, L., Wang, X., Du, M. L., Ge, C., Wang, Q. H., *et al.* (2020). Dominant protozoan species in rhizosphere soil over growth of Beta vulgaris L. in Northeast China. Bioengineered 11, 229–240. https://doi.org/10.1080/21655979.2020.1729929

530 **FIGURE LEGENDS**

531

532 **Figure 1**

533 **Cysts and telotroch Morphologies**

534 (**A, C, E, G**) Representative images of phase-contrast micrographs 0, 30 and 60 min after
535 induction of the hypo-osmotic stress: cysts (**A, E**), telotrophs (**E, G**). (**B, D, F, H**) Representative
536 images of immunofluorescence of α-tubulin (red) and DAPI staining of polylobar nuclei (blue)
537 in cysts (**B, D**) and telotrochs (**F, H**). Scale bars: 10 µm.

538

539 **Figure 2**

540 **Time-lapse imaging of excystment**

541 (**A-F**) A representative sequence of main events observed during cyst differentiation extracted
542 from the Movie 1. In this movie t=0 was undetermined. Annotation indicates the localisation
543 of the different structures : (p) papilla; (cv) CV; (c) cytophrynx; (m) oral mouth/oral cavity; (n)
544 nucleus; the dotted white line identified the location of cyst wall deformation. The
545 micrographs illustrate different interconnected steps of cyst differentiation: (**A**) the CV during
546 diastole; (**B**) the cytopharynx filling during systole; (**C**) the emergence of a thin sheet beneath
547 the papilla; (**D**) the oral cavity expansion from the thin sheet; (**E**) the cytopharynx and oral
548 cavity connexion, and the cyst wall deformation; (**F**) Basal to apical release. Scale bar: 10 µm.

549

550 **Figure 3**

551 **Kymogram of differentiation from cyst to telotroph.**

552 (**A**) Kymograph generated from Movie 2 showing the kinetics of CV pulses. Inlet shows the
553 position of the section-line selected and the localisation of CV during the first diastole
554 detected. On the kymogram are indicated : (i) the position of CV, (ii) the duration of the first
555 and second diastole detected and (iii) by vertical arrows each pulse serial number positioned
556 arbitrarily at the end of each diastole indicated (**B**) Boxplot of time for detection of a first pulse

557 (n=14). (**C**) Boxplot of number of pulses counted from t=0 to telotroch release (n=14). (**D**)
558 Mean of vacuole contraction frequencies at each pulse time series number (n=9). (**E**) Boxplot
559 of vacuole diameter: within cyst at the first (C_f) and last (C_l) pulse detected and within
560 telotroph (T) immediately after release (Fig. 3E, n=14).

561

562 **Figure 4**

563 **Time-lapse imaging of systole and cytopharynx filling**

564 (**A-D**) Static images in duplicate, without (left) and with annotation (right), and taken in Movie
565 3 at 0.4-s intervals. Images show the proximal continuity between oral mouth (M),
566 cytopharynx and CV (CV) localisation during the last systole before telotroch release. (**E**) Image
567 shows the last image before a new diastole occurs. Scale bar, 30 µm.

568

569 **Figure 5**

570 **CV punctuates the tempo of enlargement of the mouth being formed**

571 (**A, B**) images indicating how the section line was positioned to generate a kymogram. The
572 section line crosses the papilla (p), oral cavity (m), cytopharynx (c) and CV (cv). (**C**) The image
573 shows the final part of the kymogram including the last eleven contraction of the vacuole
574 before release. Horizontal dotted white bars underline the perfect synchronisation between
575 CV systole, filling of the cytopharynx and progressive and rhythmed oral cavity enlargement.
576 Bold yellow bars illustrate the opening increment of the oral cavity, perfectly rhythmed in a
577 phase pattern with the last vacuolar contractions occurring before release which is indicated
578 by the red dotted line.

579

580 **Figure 6 - Deformation and rupture of cyst wall**

581 (**A**) Time allocated to cyst wall stretching from protrusion emergence to release (n=14). (**B**)
582 Polar plot of angle between papilla position and the rupture point. Range of angles between
583 the half-line passing through the midpoint of the papilla (p; θ=0°) and the center of mass of
584 the cyst, and the half-line passing through the center of mass and the midpoint defined at the

585 site of protrusion emergence initiating the plastic deformation and then release. This range
586 only contains obtuse angle values (n=16). (**C**) Percentage of increase in cyst size resulting from
587 the ratio between the perimeters calculated at the time point just before release and before
588 protrusion occurred (n=8). (**D**) Compute curvature of a perimeter cyst just before release
589 showing local deformation of the cyst wall and the location of the papilla (p) and mouth (m).
590 Calibration bar indicates value for point curvature (μm^{-1}). (**E-J**) Phase contrast (**E-H**), DAPI
591 staining of polylobar nuclei (**F, I**) and β-actin immunostaining (**G, J**) of cysts during release.
592 Scale bars, 10 µm.

593

594 **Figure 7**

595 **Concanamycin inhibits differentiation and release**

596 (**A-D**) Phase contrast (**A, C**) and immunostaining (**B, D**) of a cyst and a teletroch with a
597 polyclonal antibody against the B1-subunit of the V1-ATPase subcomplex. (**E**) Rate of empty
598 cysts and (**F**) telotroch mean speed, at stationary phase (SP), after one hour of release in water
599 in the presence of concanamycin A (Conca A) or not (C for control). (**G**) Phase contrast and α-
600 tubulin immunostaining of representative cysts and teletrochs treated or not with
601 concanamycin A. White stars and "m" annotation indicate the CV and oral mouth position,
602 respectively. Scale bars, 10 µm.

603

604 **Figure 8**

605 **Overview of events that contribute to the formation of telotroch release from a cyst in**
606 ***Vorticella microstoma***

607 A step-by-step schematic diagram of a cyst/telorotroch transition depicting the hypothesis
608 raised in this work according to which within the cyst, the papilla position at the wall cyst
609 and a functional contractile vacuole cause and orient organelles formation (cytopharynx and
610 ciliated oral mouth) as well as apical-basal telotroch polarity, and subsequent telotroch
611 release.

612

613 **Supplementary Figure 1**

614 **Telotroch Release from cyst**

615 Micrographs of six cysts and telotrochs at t=0 (left) and approximately t=50 min (right) just
616 after release. (p) indicates the papilla localisation, and (*) the position where the cyst wall will
617 be (left) and is ruptured (right). The apical-basal polarity of telotrophs is indicated immediately
618 after release illustrating that excystment involves a specific orientation of telotrophs in the
619 opening of the cyst wall with the basal end at first and then the apical end (easily identified by
620 the oral cavity). Scale bar: 20 µm.

621

622 **Supplementary Figure 2**

623 **Kinetics of vacuole beat frequency as a function of the ordered series of diastole-systole**
624 **cycles**

625 Nine independent time-lapse experiments recording cysts from t=0 to the release time
626 ranging between 20 and 40 min. X-axis indicates the serial number of cycles; y-axis is
627 indicative of the beating frequency between two successive pulses.

628

629 **Supplementary Figure 3**

630 **α-tubulin staining of cells treated or not treated with concanamycin A**

631 (**A-B**) Merged images of phase contrast and α-tubulin immunostaining of representative cysts
632 and teletrochs treated (**B**) or not (**A**) with concanamycin A. Scale bar: 50 µm. (**C-G**) typical
633 timing of systole duration of 1s with the dynamics of engulfment of the cytopharynx and
634 emergence of oral cavity signed by membrane invagination below the papilla. (**H-L**) Extension
635 of systole duration (7s) with no structures reminiscent to the cytopharingal cavity nor cilated
636 oral mouth in a concanamycin A-treated cyst connection. Scale bar: 10 µm.

637

638

639

640 **Movie1 - Time-lapse video microscopy of a cyst differentiating in a telotroch**

641 Images were taken every 500 ms with a 40× objective. t=0 was undetermined. Annotation
642 recordings is frame-by-frame.

643

644 **Movie2 - Video microscopy of a cyst differentiating in a telotroch**

645 Time-lapse imaging with 0.4-s intervals. Images were taken every 400 ms with a 40× objective.
646 The indicated timing is refered to t=0 when the differentiation started in response to hypo-
647 osmotic conditions.

648

649 **Movie3 - Video microscopy of a cyst differentiating in a telotroch**

650 Images were taken every 200 ms with a 40× objective. The indicated timing is refered to t=0
651 when the differentiation started in response to hypo-osmotic conditions.

652

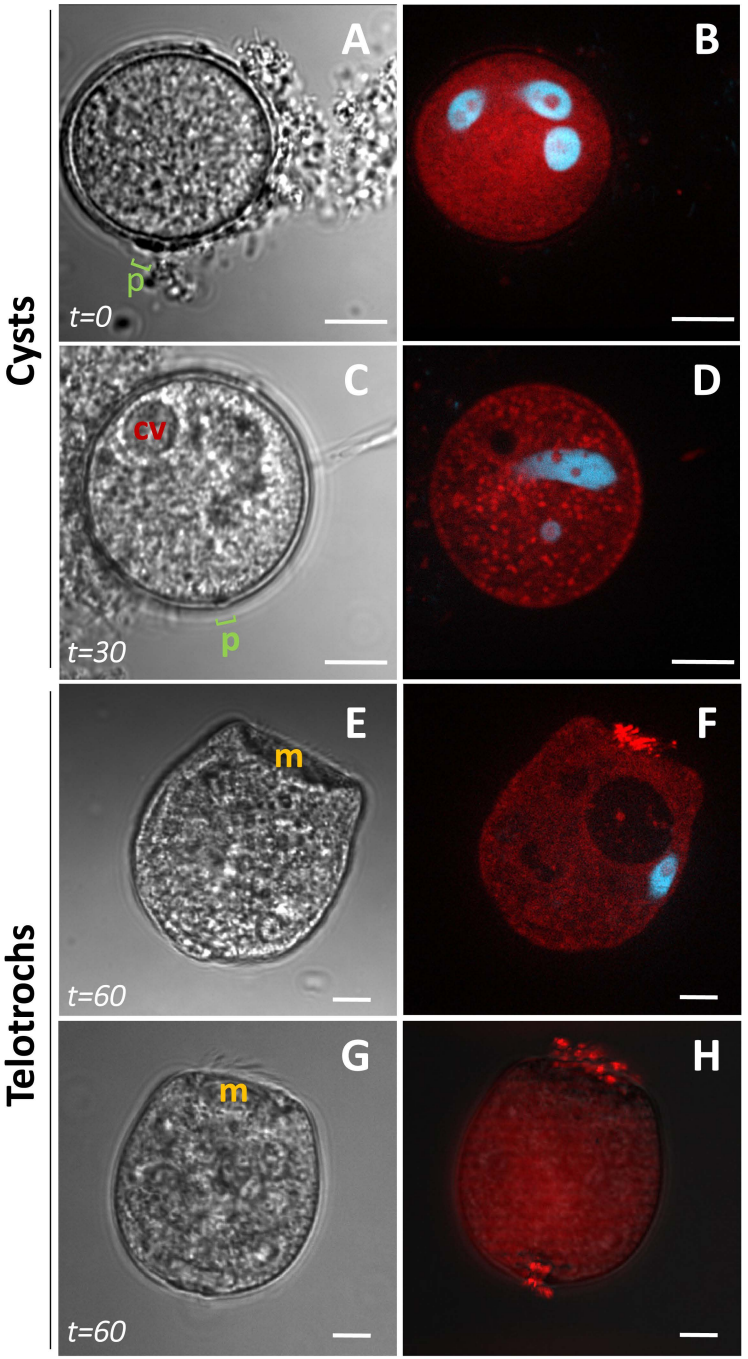

Figure 1

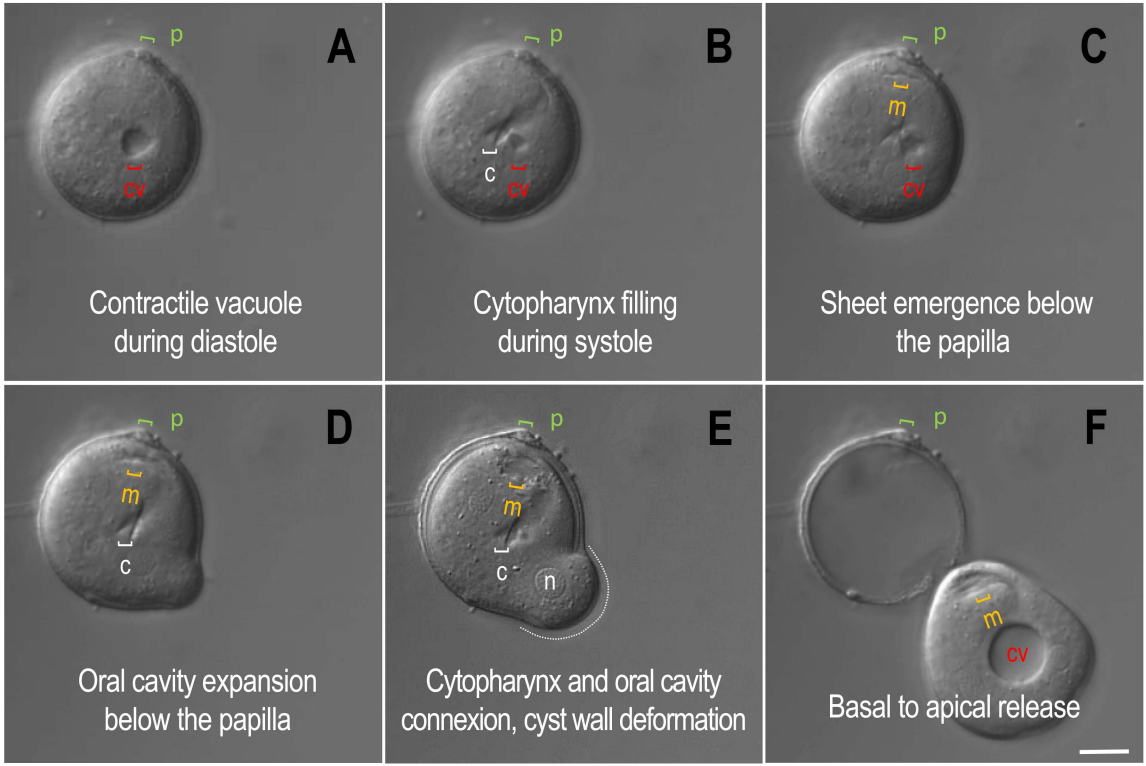
A
p
cv
Contractile vacuole during diastole
B
p
c
cv
Cytopharynx filling during systole
C
p
m
cv
Sheet emergence below the papilla
D
p
m
c
Oral cavity expansion below the papilla
E
p
m
c
n
Cytopharynx and oral cavity connexion, cyst wall deformation
F
p
m
cv
Basal to apical release

Figure 2

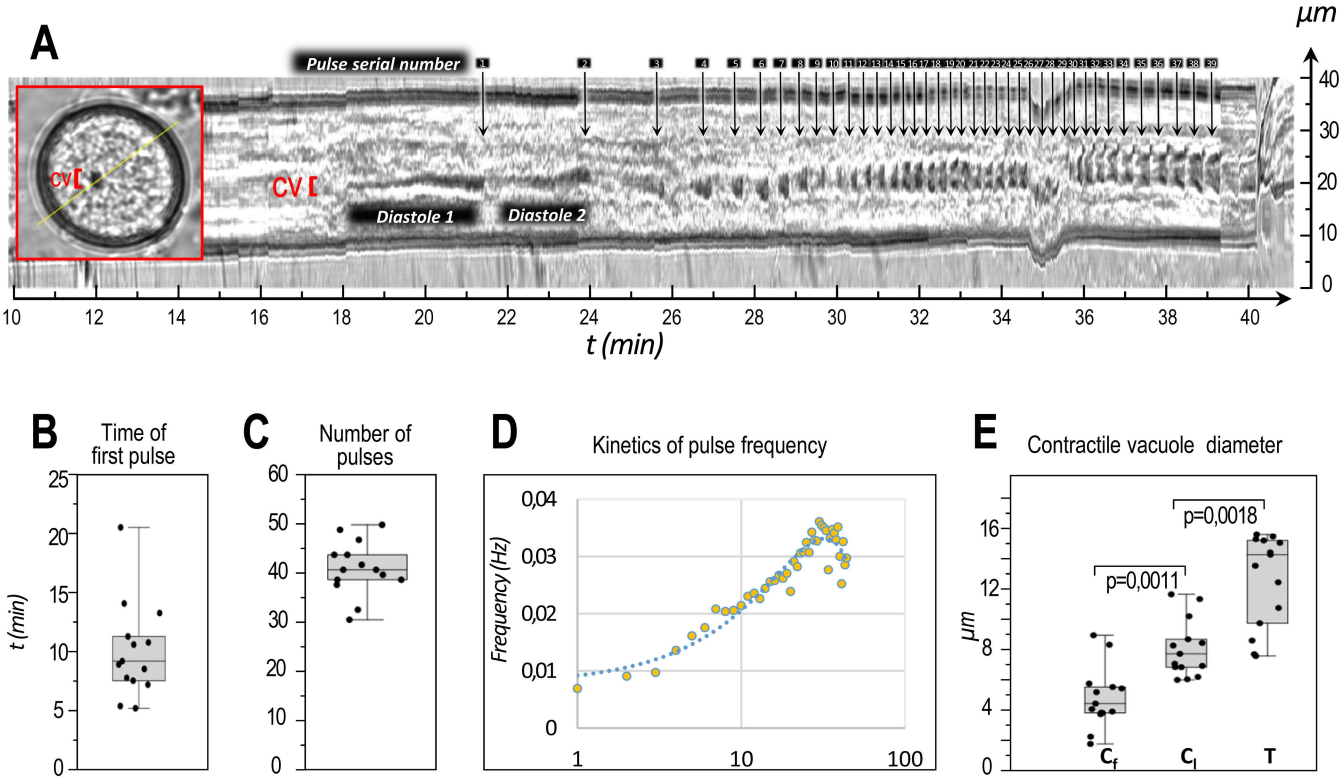
A
Pulse serial number
CV
CV
Diastole 1
Diastole 2
µm
t (min)
B
Time of first pulse
t (min)
C
Number of pulses
D
Kinetics of pulse frequency
Frequency (Hz)
E
Contractile vacuole diameter
µm
p=0,0011
p=0,0018
C_f
C_l
T

Figure 3

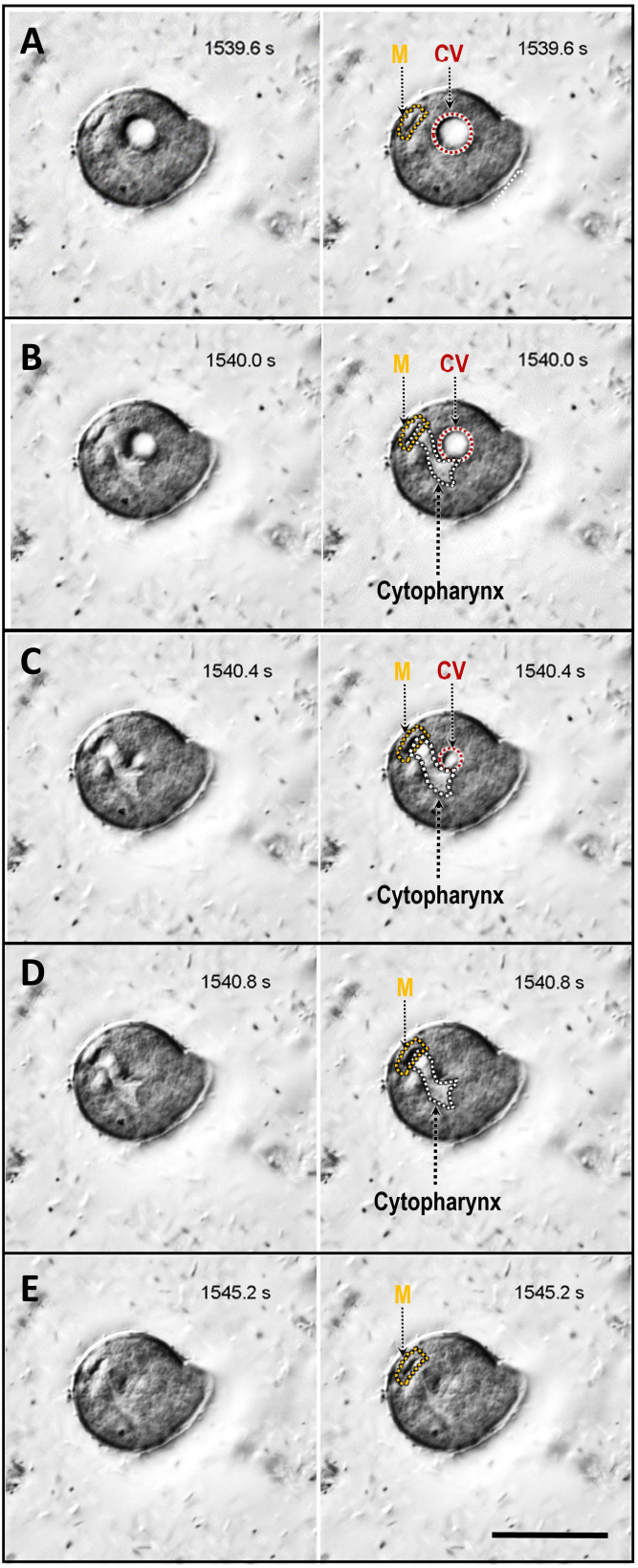
A
1539.6 s
M
CV
1539.6 s
B
1540.0 s
M
CV
1540.0 s
Cytopharynx
C
1540.4 s
M
CV
1540.4 s
Cytopharynx
D
1540.8 s
M
1540.8 s
Cytopharynx
E
1545.2 s
M
1545.2 s

Figure 4

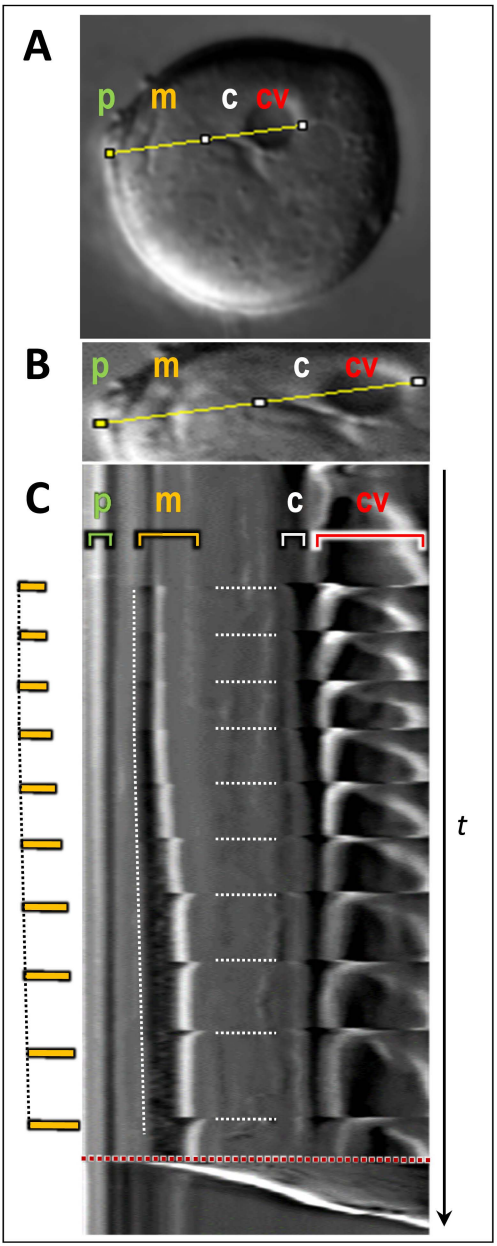

Figure 5

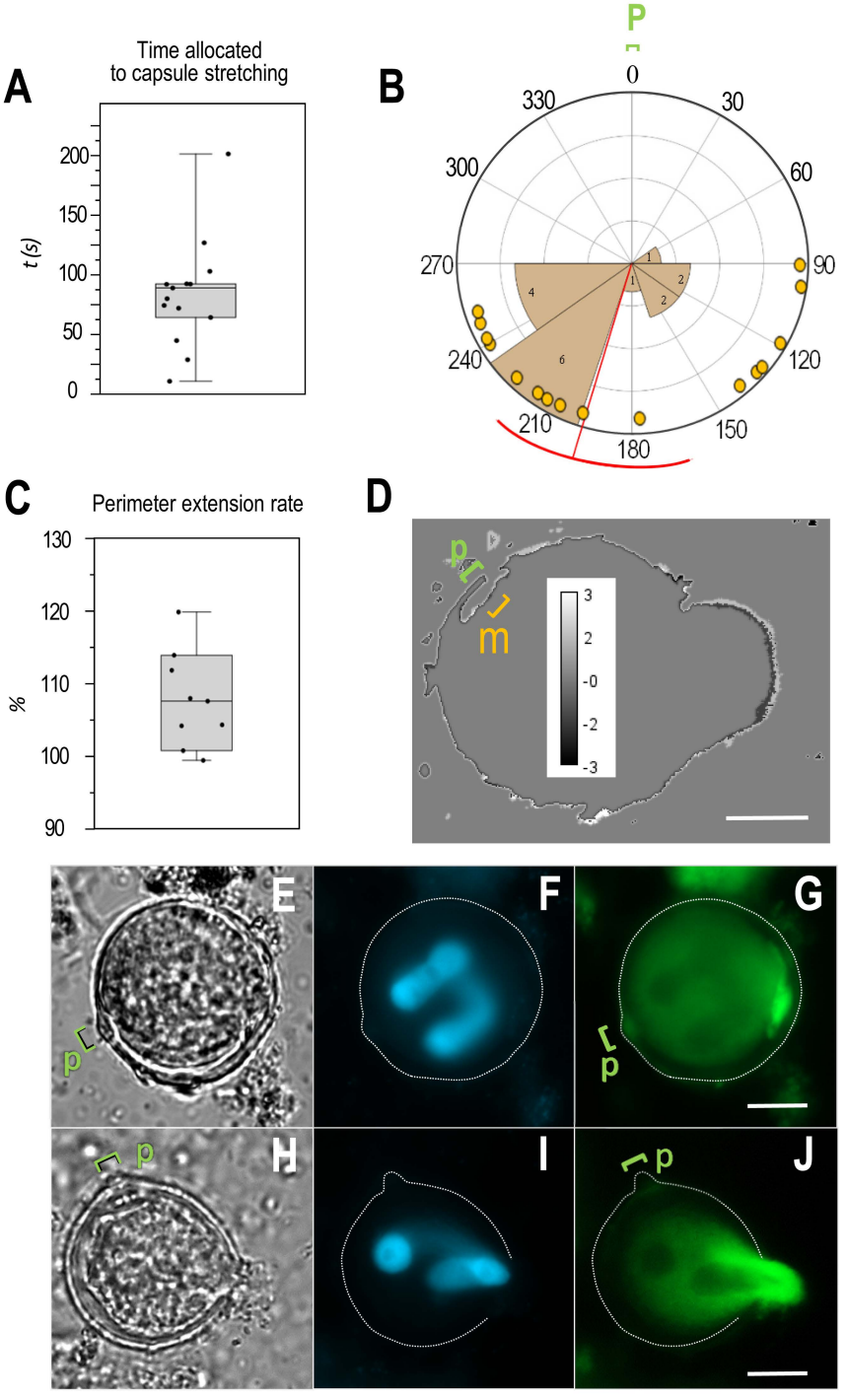
A
Time allocated
to capsule stretching
t (s)
200
150
100
50
0
B
P
0
30
60
90
120
150
180
210
240
270
300
330
1
2
4
6
C
Perimeter extension rate
%
130
120
110
100
90
D
p
m
3
2
-0
-2
-3
E
F
G
H
I
J
p

Figure 6

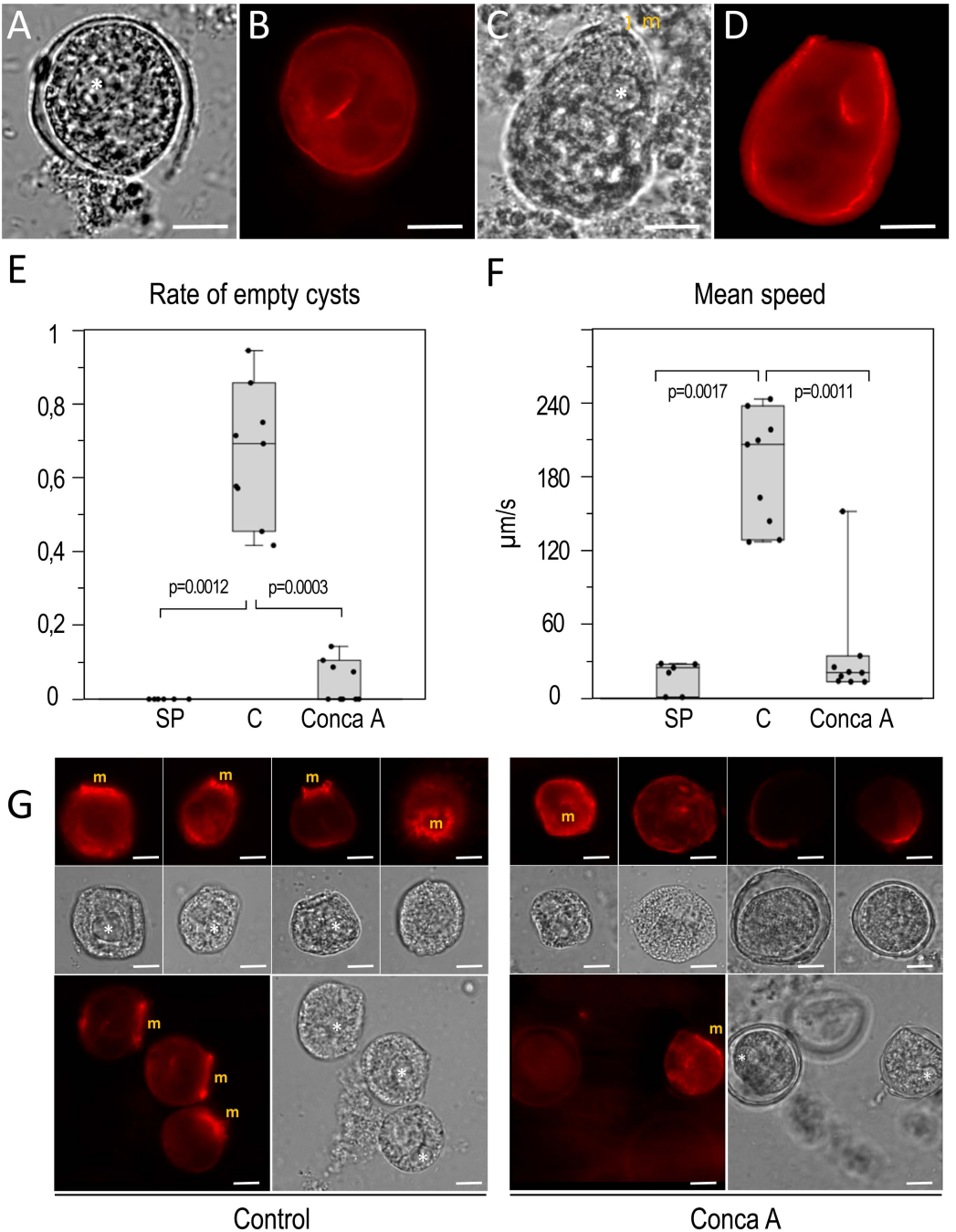
A
B
C
1 m
D
E
Rate of empty cysts
1
0,8
0,6
0,4
0,2
0
p=0.0012
p=0.0003
SP
C
Conca A
F
Mean speed
240
180
120
60
0
µm/s
p=0.0017
p=0.0011
SP
C
Conca A
G
m
Control
Conca A

Figure 7

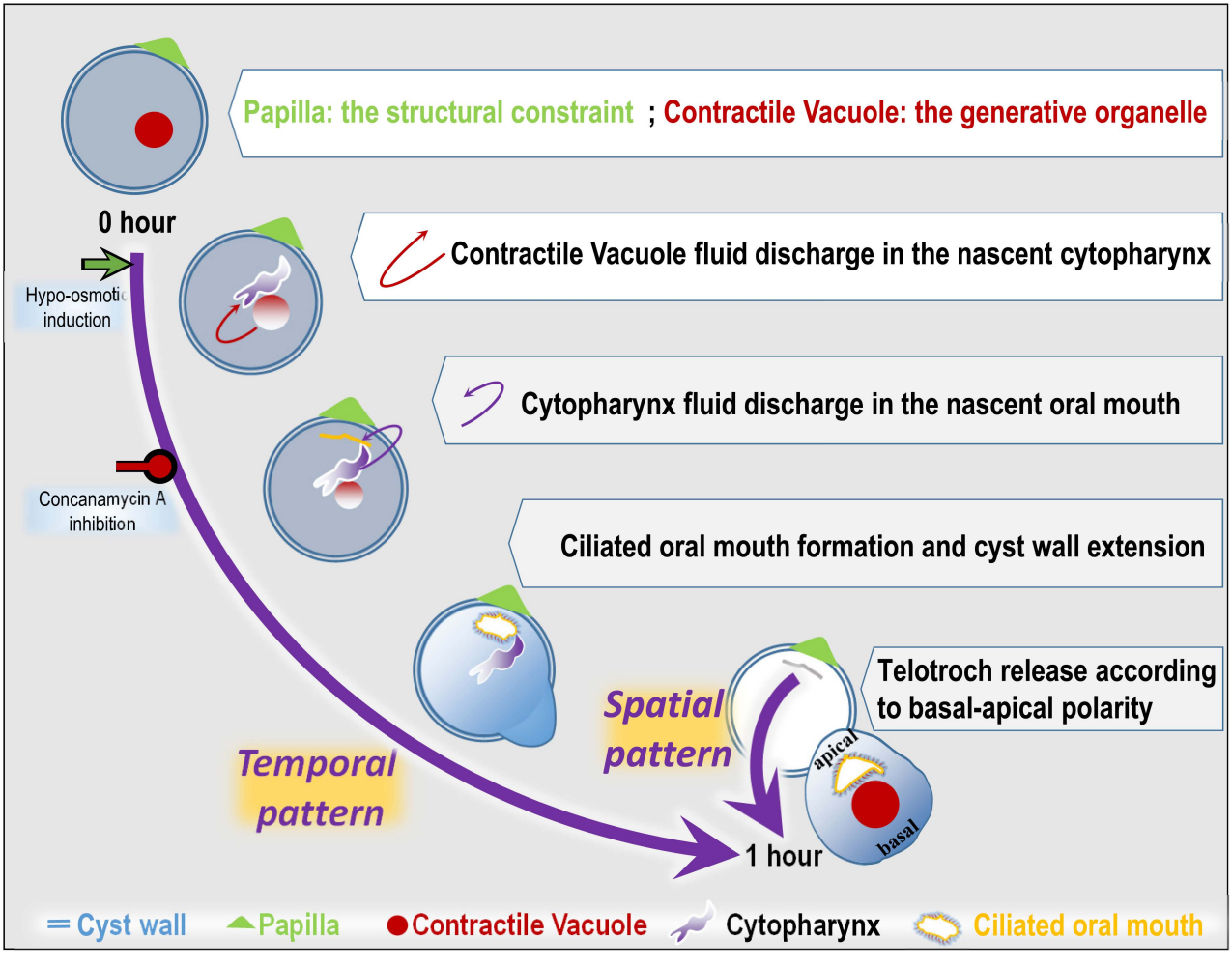
Papilla: the structural constraint ; Contractile Vacuole: the generative organelle
0 hour
Hypo-osmotic induction
Contractile Vacuole fluid discharge in the nascent cytopharynx
Cytopharynx fluid discharge in the nascent oral mouth
Concanamycin A inhibition
Ciliated oral mouth formation and cyst wall extension
Telotroch release according to basal-apical polarity
Spatial pattern
Temporal pattern
apical
basal
1 hour
Cyst wall
Papilla
Contractile Vacuole
Cytopharynx
Ciliated oral mouth

Figure 8